Journal of Innovative Optical Health Sciences
Vol. 4, No. 2 (2011) 199–208

DOI: 10.1142/S1793545811001459

MR-GUIDED PULSE OXIMETRY IMAGING OF BREAST *IN VIVO*

ZHIQIU LI, SHUDONG JIANG, VENKATARAMANAN KRISHNASWAMY,
SCOTT C. DAVIS, SUBHADRA SRINIVASAN,
KEITH D. PAULSEN and BRIAN W. POGUE*
Thayer School of Engineering, Dartmouth College
Hanover NH 03755, USA
**Brian.Pogue@dartmouth.edu*

A near-infrared (NIR) tomography system with spectrally-encoded sources in two wavelength bands was built to quantify the temporal oxyhemoglobin and deoxyhemoglobin contrast in breast tissue at a 20 Hz bandwidth. The system was integrated into a 3 T magnetic resonance (MR) imaging system through a customized breast coil interface for simultaneous optical and MRI acquisition. In this configuration, the MR images provide breast tissue structural information for NIR spectroscopy of adipose and fibro-glandular tissue in breast. Spectral characterization performance of the NIR system was verified through dynamic phantom experiments. Normal human subjects were imaged with finger pulse oximeter (PO) plethysmogram synchronized to the NIR system to provide a frequency-locked reference. Both the raw data from the NIR system and the recovered absorption coefficients of the breast at two wavelengths showed the same frequency of about 1.3 Hz as the PO output. The frequency lock-in approach provided a practical platform for MR-localized recovery of small pulsatile variations of oxyhemoglobin and deoxyhemoglobin in the breast, which are related to the heartbeat and vascular resistance of the tissue.

Keywords: High frame-rate; fast imaging; MR-guided; near-infrared tomography; breast hemodynamics.

1. Introduction

Near-infrared spectral tomography has been extensively studied to measure functional properties of breast tissue, with an aim of providing fundamental insight or diagnostic information about breast cancer management.[1] While diffuse spectroscopy of tissue has an inherently low spatial resolution as a direct result of the multiple scattering of photons passing through several centimeters of tissue,[2] recent advances in system integration with clinical imaging modalities, including X-ray mammography,[3] ultrasound,[4] X-ray tomosynthesis,[5] and magnetic resonance imaging,[6,7] have shown that the spatial resolution may not be entirely limited if the focus is developed around NIR spectroscopy of predefined volumes. In addition, dynamic contrast mechanisms, such as those from optical contrast agent pharmacodynamics or from gas inhalation changes, induce rapid vascular changes in breast tissue[8,9] and are under exploration to improve image contrast and specificity. These functional contrast changes have induction curves, which change rapidly over seconds and minutes and thus require faster imaging systems to capture the physiologically critical information about vascular dynamics and resistance with biologically accurate temporal resolution. This study presents the development of a fast MR-guided multispectral band NIR tomography

*Corresponding author.

system with high temporal resolution, which was tested in human breast imaging.

Currently, most multi-spectral NIR imaging systems acquire data at far slower rates than is required for capturing important dynamic changes in tissue as most systems used in clinical trials require several minutes to acquire one image. A few techniques have been proposed to image at sub-second timescales, among which was one based on frequency modulation to encode each wavelength of the light source,[10,11] or the spatial position of the source light[12] in order to reduce or eliminate sequential source switching. This imaging technique is flexible and can achieve imaging rates as high as 150 Hz,[11] and it is especially suitable for small subjects such as rats. However, the dynamic range required to image larger tissue volumes, such as human breast, places severe limitations on accumulating enough signal from multiple sources around the tissue at each detector. Ultimately, it is not possible to detect signals with widely varying dynamic range in the same detector. The imaging speed of most systems degrades drastically with tissue thickness and longer minimum exposure times are required to accumulate enough signal on the detector. Therefore, the maximum speed reported for routine breast imaging has been 3 Hz, yet most reported clinical trial summaries have been carried out on systems with acquisition times of several minutes. But imaging at speeds much faster than the tissue activity rate of interest, such as heartbeat rate, is important to provide quantitative information on physiological dynamics, and could potentially allow the use of signal processing methods to improve the signal-to-noise ratio.

In earlier work, a scheme to use spectrally-encoded laser diodes (LD) centered around 785 nm for continuous-wave (CW) tomography through small objects was demonstrated and achieved imaging frame rates of 30 Hz.[13] The interface and detection part of this system was modified to improve the dynamic range of the detectors and allow imaging through breast tissues, up to 7−8 cm thickness, with a 20-Hz acquisition rate.[14] Guided by the tissue structural information from MR images and the locking frequency reference from a pulse oximeter (PO), the improved system demonstrated the ability to recover temporal variations in absorption coefficient μ_a in the breast tissue of a healthy female subject.[15]

In this present study, an additional set of seven 830-nm laser diode sources has been incorporated into the high-speed NIR system to form a second wavelength band, which allows spectroscopic interpretation without decreasing the acquisition frame rate of the system. The potential application for this high-speed two-wavelength tomography system is to monitor the temporal concentrations of oxyhemoglobin (HbO) and deoxyhemoglobin (Hb), and convert these values to total hemoglobin (Hb_T) and oxygen saturation (SO_2) signals within the breast *in vivo*, which are critical parameters for breast tumor diagnosis.[16] In this study, the performance of the system was verified through a series of phantom experiments, and a human case study was completed with a healthy volunteer to show the system's ability to reveal the hemodynamics of breast adipose and fibroglandular tissues.

2. System Configuration

The dual-wavelength system consists of a source cart, a detection cart, and a phantom/tissue interface as shown in Fig. 1. The detection system and the tissue interface are identical to those of the single-wavelength video-rate tomography system previously reported.[14] In addition to the original seven 785-nm band LDs, another set of seven LDs with a central emission wavelength at 830 nm were installed onto the source system. LDs within each wavelength band (785 or 830 nm) were carefully tuned with the accompanying temperature and current control circuits to achieve about 1 nm separation in between each, and stable enough for a 20-min imaging session. The 1,200 grooves/mm gratings of the seven CCD-based spectrometers (Acton, MA, USA) on the detection cart were set to be centered at 805 nm, so that signals from all LDs of both wavelength bands can be resolved on the CCDs simultaneously. All spectrometers were hardware synchronized and controlled by a custom-developed LABVIEW program on a console computer. The breast/phantom interface is comprised of two parallel plates, with sources and detection fibers positioned across from one another in a purely transmission mode arrangement, as shown in Fig. 1. This configuration minimizes the overall dynamic range, allowing all transmitted signals to be measured with a fixed exposure time setting on all the CCDs. It was found that the signal-to-noise in acquisition would not be affected by the acquisition speed, as long as the signal amplitude was kept constant. Therefore the imaging speed was always

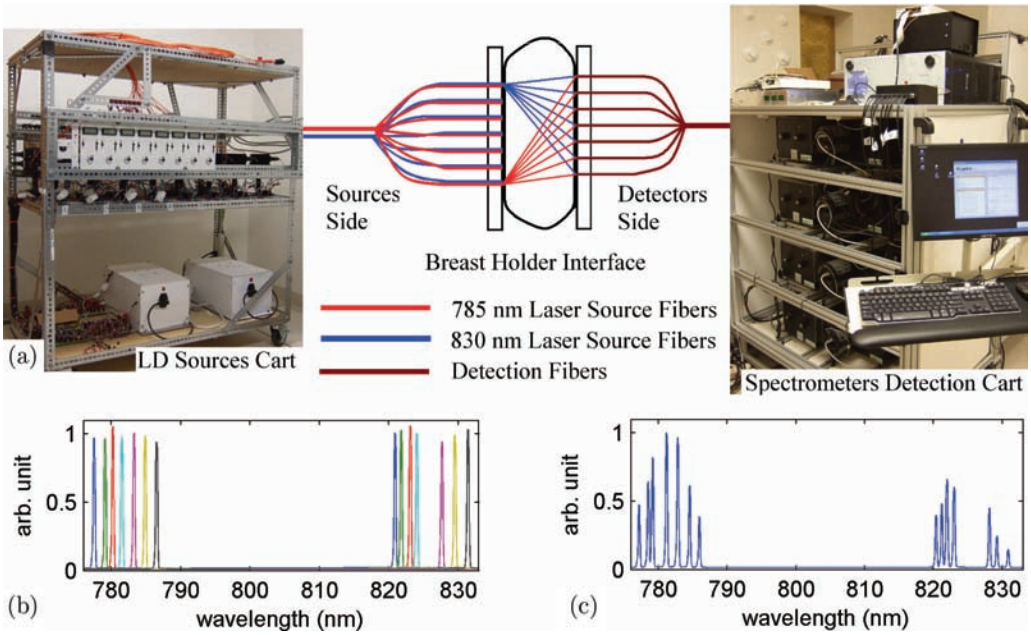

Fig. 1. (a) The configuration of the dual-band NIR tomography system is shown. The source cart housing 14 laser diodes (in two bands of seven lasers each) and accompanying circuits is on the left, and the detection cart housing seven spectroscopy systems and a console computer is on the right. The diagram of the phantom/tissue interface and illustrative light paths is in the middle. (b) The normalized intensities of LDs before transmission into the tissue. (c) The normalized intensities of LDs on one CCD after passing through a 63-mm breast tissue phantom.

chosen to be as low as possible in order to maximize the exposure time and thus maximize signal intensity on the CCDs, while avoiding saturation. The system typically runs at 10 to 25 Hz, depending on the optical properties and the thickness of the media, while the maximum imaging speed of this system is ∼60 Hz.

3. Phantom Experiments and Results

3.1. *Validation of hemoglobin concentration recovery in phantom tests*

A tissue-simulating phantom with thickness of 63 mm and lateral dimension of 120 mm was made from agarose powder, intralipid, porcine whole blood and phosphate buffered saline (PBS), according to a previously published procedure,[17] and is pictured in Fig. 2. The 0.75% intralipid concentration of the phantom resulted in a reduced scattering coefficient μ_s' of 0.76 mm^{-1} at 785 nm and 0.72 mm^{-1} at 830 nm.[18] Hb_T was set to 15 μM in the phantom, which is within the normal range for Hb_T level in human breast tissue. SO_2 of the phantom were close to 100%, because of the fresh

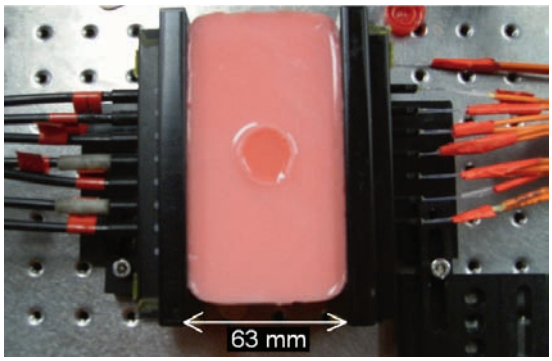

Fig. 2. The agarose phantom with a liquid anomaly in the middle, used to vary hemoglobin levels in a single inclusion. The light sources were guided by the orange fibers on the right, and the black detection fibers on the left were connected to the spectrometer/CCDs.

porcine whole blood used in making the phantom. The phantom included a cylindrical anomaly of 20 mm diameter in the middle of the phantom. The anomaly was first filled with a solution of 15 μm Hb_T and 0.75% intralipid to make the phantom optically homogeneous, and a measurement was made. Then the solution in the anomaly was withdrawn with a syringe, and the anomaly was filled with a batch of solutions of increasing Hb_T and constant 0.75% intralipid concentration. One measurement was

made for each new solution. The Hb_T of the solution batch increased from 15 to 40 μM.

After compensating for the intensity of the different lasers and the efficiency of the detectors, each dataset was calibrated with the homogeneous measurement. A 2D slab-shaped mesh of 5,249 nodes was created and segmented into the anomaly region and the background region corresponding to the exact dimensions of the phantom. Then a region-based reconstruction algorithm[15] was applied to the datasets, fitting for oxyhemoglobin and deoxyhemoglobin values. The results from a systematic increase in hemoglobin and corresponding fits are shown in Fig. 3.

The SO_2 of both the background and the anomaly had small fluctuations, with approximately 2% standard error (standard deviation normalized by the mean value). The reconstructed Hb_T of the background remained constant and agreed very well with the true value of 15 μM. The Hb_T of the anomaly agreed with the true value for lower Hb_T solutions, but was slightly overestimated with increased Hb_T in the anomaly region. Local variations in total hemoglobin in the anomaly liquid could also be a cause for this. However, the largest absolute error was only 8.3% in the 35 μM case, which is reasonable for breast imaging with this system, especially given there are only two wavelength bands and relatively narrow spectrum coverage.

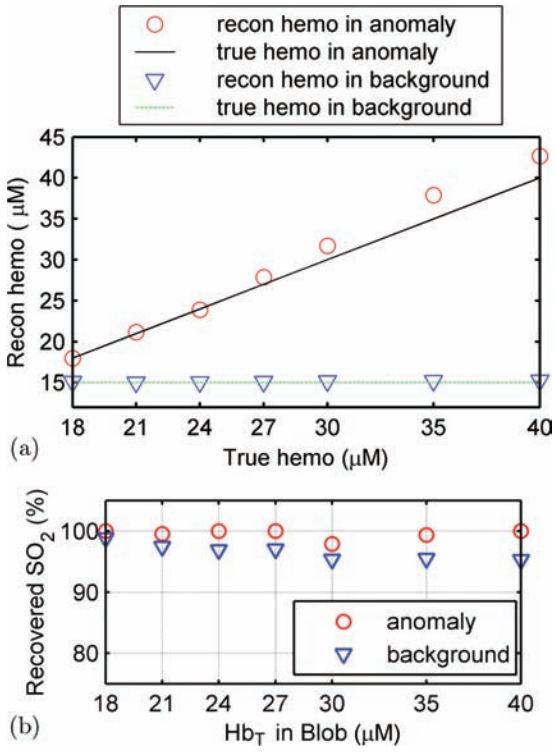

Fig. 3. (a) The reconstructed and true total hemoglobin (Hb_T) in the anomaly region and the background are plotted, showing the expected linear and flat trends. (b) The reconstructed SO_2 in the anomaly and the background are shown, with less than 2% standard error in both cases.

3.2. *Validation of hemoglobin oxygen saturation recovery in phantom tests*

To verify the system's ability to recover SO_2, especially at high speed, a deoxygenation experiment with yeast was carried out. An agarose slab phantom identical to the one in Fig. 2 was made and used as the background, while the anomaly in the middle was filled with solution of high Hb_T concentration and 0.75% intralipid. A reflectance-based tissue oximeter (T-Stat 303, Spectros Corporation, Portola Valley, CA, USA) was set up to monitor the SO_2 in the anomaly simultaneously with the NIR system, as shown in Fig. 4. The tissue oximeter utilizes a reflectance signal from the visible wavelength range of 420 to 700 nm for hemoglobin oxygenation spectral fitting, so its signal was filtered out by the grating on the NIR system and did not contaminate the NIR signal on the detector, allowing both to operate at the same time. Yeast was added to the liquid anomaly region and mixed well immediately before measurements were recorded. The tissue oximeter sampled at 1 Hz, while the sampling period of the NIR system was 60 ms. The entire deoxygenation experiment lasted for 10 min before the SO_2 reading of the tissue oximeter settled to a constant value near 5% saturation, effectively showing the minimum value detectable for desaturation.

The NIR data was calibrated and reconstructed frame by frame. The reconstructed SO_2 of the solution in the anomaly was plotted together with the reading from the tissue oximeter in Fig. 5. Compared with the reading of the tissue oximeter, the slope of the SO_2 curve of the NIR system was less steep, and the reading was slightly underestimated above 52% saturation and overestimated below this level. For most clinical applications where SO_2 was usually above 40%, the difference of these two modalities was within a maximum of 10% difference.

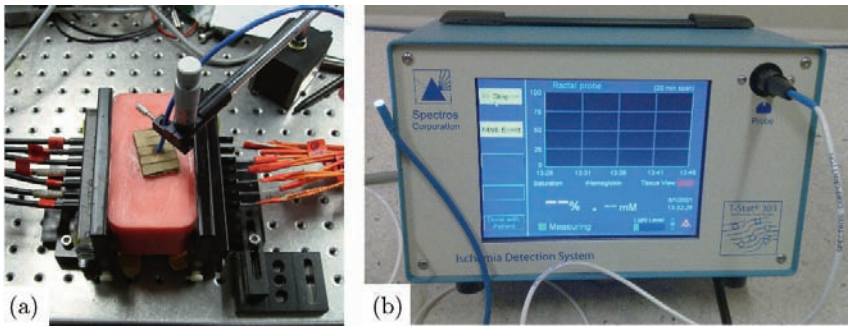

Fig. 4. (a) The setup of the deoxygenation experiment is shown, with the blue probe of the reflectance tissue oximeter extended into the anomaly in the phantom. (b) The reflectance tissue oximeter interface.

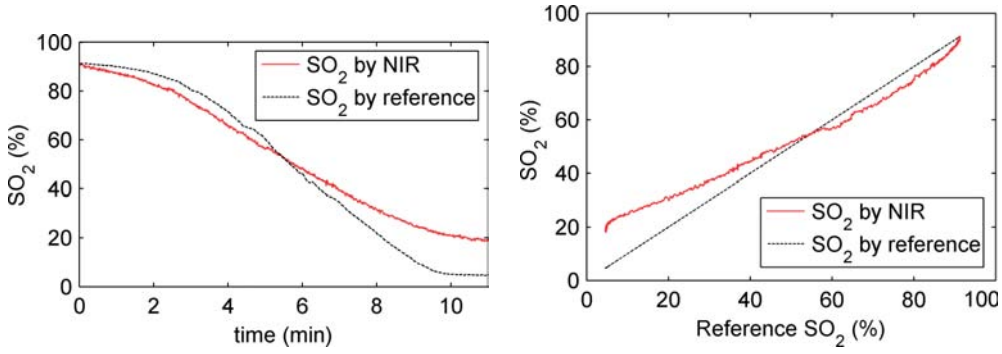

Fig. 5. (a) The SO_2 readings from the two modalities (visible reflectance probe *reference* and spectrally-encoded *NIR* tomography) versus time of the experiment are shown. The same data is replotted in (b) for SO_2 from NIR tomography versus SO_2 by reflectance probe reference.

4. Human Breast Imaging

The experimental setup for breast imaging is shown in Fig. 6. A healthy female volunteer was recruited for the imaging experiment. In addition to the NIR data, MR images are essential to provide breast shape and tissue structure information for the region-based reconstruction algorithm (www.nirfast.org). To minimize the co-registration error, MR images were collected simultaneously with the NIR data during patient imaging. To realize this, both

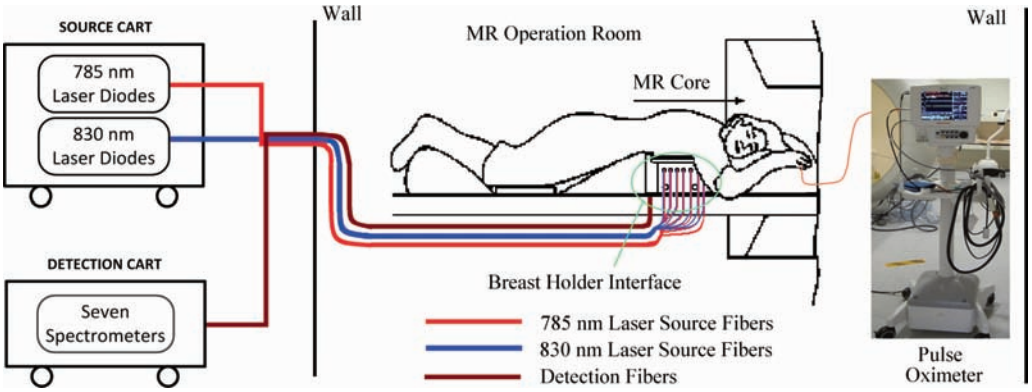

Fig. 6. The experimental setup for breast imaging inside the MRI, shows the laser diodes and spectrometers (left) with fiber coupling into the MRI system (center). Data collection was synchronized with finger pulse oximetry (right) to monitor pulsatile flow data in a frequency-locked manner.

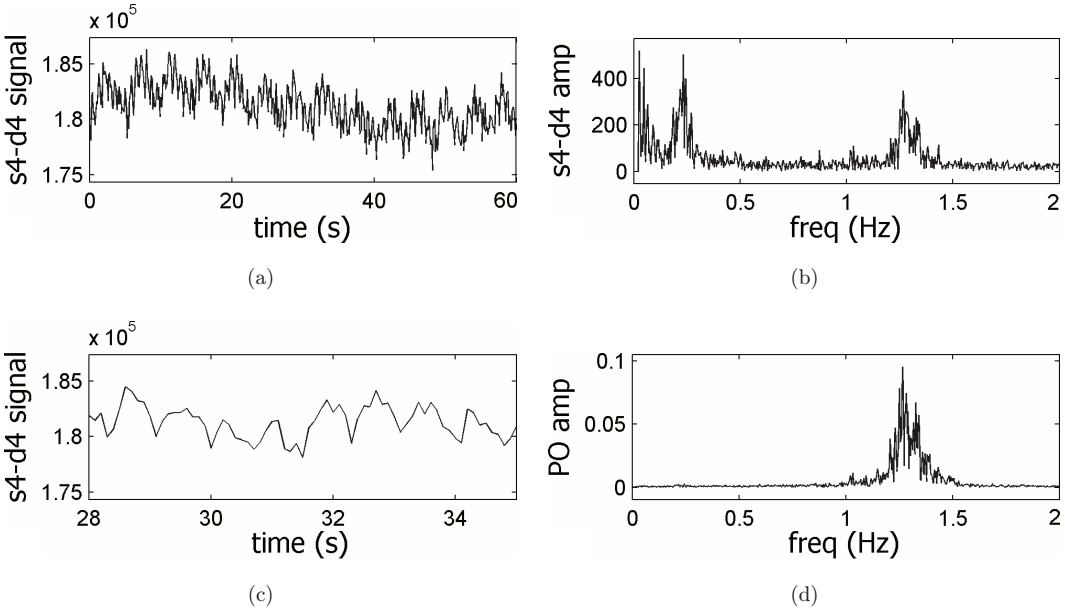

Fig. 7. In (a) the raw data from the 4th detector and the 4th laser source, is shown in the time domain, and in (b) is the Fourier transform of (a). In (c) part of (a) is zoomed in and shown with periodic signal component related to heartbeat. In (d) is the Fourier transform of the output of finger PO signal.

the source fibers and the detector fibers were extended into the MR room and fixed onto the breast interface, which was in turn fixed inside a customized breast MR coil. Co-registration of the two imaging modalities was realized by MR fiducials on the breast interface. The subject lay prone on the breast coil on the MRI bed, with the right breast gently compressed into a 52-mm thick slab shape by the breast interface. The thickness of 52 mm was chosen for this breast so that the compressed breast width matched the array of sources and detectors on the breast holder, while the compression resulted in no pain to the subject.

The finger pulse of the subject was also continuously monitored during the imaging session by a MR-compatible pulse oximeter (PO, Veris Vital Signs Monitor, MEDRAD, Inc.) to provide a frequency-locking reference to the NIR dataset. The PO produces a continuous analog signal output proportional to the detected optical signal on the finger, allowing sampling with a DAQ board on the same computer that controls the NIR system and at the same rate as the NIR system, which was 20 Hz in this human breast imaging exam. The scout scans, T1-weighted and T2-weighted coronal scans took the MR system 15 min in total to complete. The NIR system and the PO acquired measurements for 134 sec.

A 0.2−0.3 Hz periodic component was observed in the raw data of all detectors, which was likely caused by the respiration of the subject. The raw data at the 4th detector from the 4th 785 nm source was shown in Fig. 7(a) as an example. In addition, the Fourier transform of the raw data [Fig. 7(b)] also showed a smaller peak around 1.3 Hz. This frequency component became obvious in Fig. 7(c), which is part of Fig. 7(a) after being zoomed in. This frequency component was verified to be caused by the heartbeat, using the Fourier transform of the PO output, as shown in Fig. 7(d). The same pattern was found in other source-detector pairs, as well as in the raw data from the 830-nm wavelength band, which verified that this NIR system could detect the small fluctuation of optical signal caused by both breathing and heartbeat.

Because the hemodynamics in breast tissue is more related to the heartbeat, the frequency component related to breathing was filtered out from the raw data first. The data were compensated with source intensities and detector efficiencies and calibrated per wavelength band with the measurement on a slab-shaped homogeneous agarose phantom to remove coupling offset as described in detail previously.[14] The mesh for reconstructing the optical data was created from the coronal MR scan images. Figure 8(a) is a coronal T1 MR image of the breast.

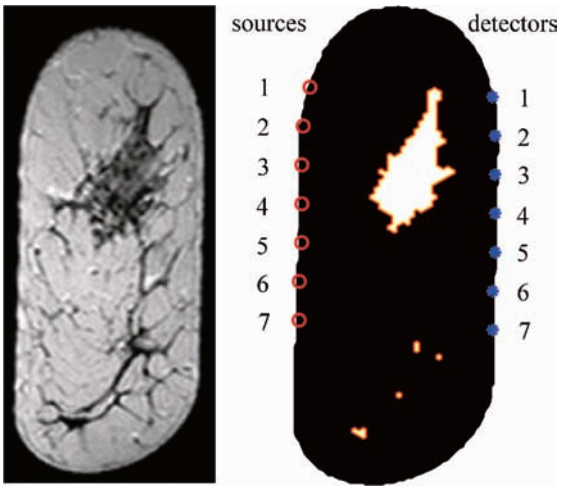

Fig. 8. (a) The inplane coronal slice of the T1-weighted MR image is shown for the right breast of the subject imaged. This image was used to create a mesh with segmentation of the adipose tissue (black) and the fibroglandular tissue (white) in (b). The positions of source and detector fibers are marked accordingly with circles.

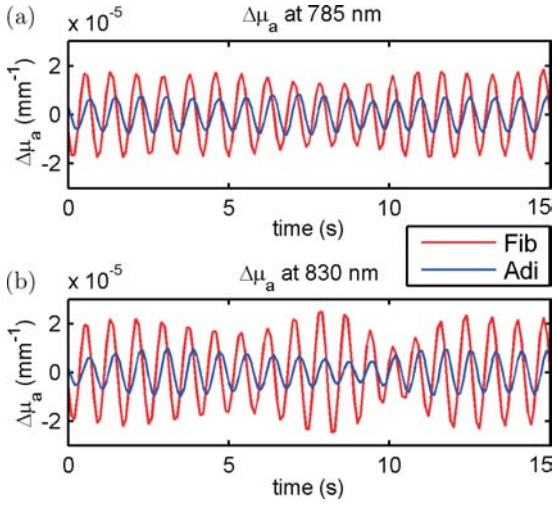

Fig. 9. The change in μ_a of the two tissue types are shown at 785 nm (a) and 830 nm (b). These were estimated by region-based recovery in the inversion algorithm.

The dark region inside the tissue is composed mostly of fibroglandular tissue which typically contains higher hemoglobin content, while the gray region is mostly adipose or fatty tissues which generally have lower hemoglobin content.[7] From the MR image, a 2D mesh with 3,963 nodes was created and segmented into two regions, e.g., the fibroglandular region and the adipose region, as shown in Fig. 8(b), to perform region-based optical spectroscopy. This reconstruction algorithm is based on the finite element model of the diffusion equation and groups all nodes into two tissue types and thus results in homogenous μ_a value inside each region. This algorithm is more robust against experimental noise and is more convenient to compare the hemodynamic characteristics of different tissue types.[15]

Because the laser sources of the NIR system work in continuous wave mode, there is no ability to separate absorption coefficient, μ_a, from scattering, μ_s', in the images. However extensive earlier work with a frequency domain system has led to reasonable estimates for the μ_s' values for adipose and fibroglandular tissues, which appear to be stable to within 15% between subjects.[7] These values are $\mu_s'(adip) = 0.60\ \text{mm}^{-1}$ in the adipose region and $\mu_s'(fibro) = 1.00\ \text{mm}^{-1}$ in the fibroglandular region for 785 nm, and $\mu_s'(adip) = 0.55\ \text{mm}^{-1}$ and $\mu_s'(fibro) = 0.95\ \text{mm}^{-1}$ at 830 nm.

Assuming the above values for scattering coefficients, μ_a of each wavelength band was reconstructed separately and frame by frame on a desktop computer. A data stream of total length 15 s is shown, for μ_a values at the two wavelengths in Fig. 9. The plot suggests that the temporal μ_a showed a period of about 1.3 Hz for both tissue types and both wavelength bands. The mean value and the variation of μ_a are larger in the fibroglandular region than in the adipose region, which agrees with common physiological knowledge and previous studies.[7] The value of μ_a at 830 nm is slightly larger than that of 785 nm in both tissue types, which agrees with the expectation that HbO makes up the larger fraction of blood in the pulsatile signal, and has a higher absorption coefficient at 830 nm than at 785 nm.

To verify the temporal resolution of μ_a of the NIR system, the temporal frequencies of recovered μ_a in two tissue types were compared to the analog output of the PO, and the raw data at the 4th detector from the 4th 785-nm source after removing the frequency component related to breathing. For each dataset, an FFT was performed on every 10 s of the dataset, and the peak frequency was recorded as the main frequency of this segment. This process was repeated with the increment of 1 s step size. The curves of peak frequencies along the time were plotted in Fig. 10. The general shapes of those four curves were identical, which illustrates that the NIR system could capture very similar temporal changes in μ_a as the PO did. The curves of two tissue types and the raw data was exactly in phase, meaning they were driven by the same heart pulse. Despite the identical shapes, the curve of PO has about 4 s

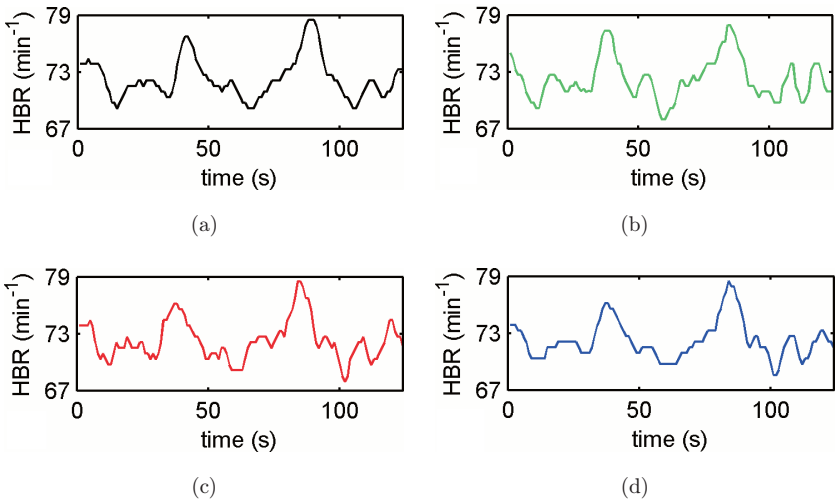

Fig. 10. (a) The peak frequency of the pulse oximeter output along the time. (b) The peak frequency of the 785 nm signal going from the 4th detector to the 4th source, after removing the frequency component related to breathing. (c) The peak frequency of μ_a of the fibroglandular region at 785 nm band along the time. (d) The peak frequency of μ_a of the adipose region at 785 nm band along the time.

lag compared to the other three. This is probably due to the smoothing and data processing algorithms inside the PO. The curves at 830 nm band were identical to those at 785 nm band, and thus were not listed here.

5. Discussion

The purpose of this system development and testing was to establish whether hemodynamics could be tracked through thick breast tissue with MR guidance. Previous work with the system was done with a single wavelength, and so the addition of a second wavelength band provides the ability to estimate oxygen saturation changes at a high frame rate. There are a number of ways that dynamic vascular contrast can be examined by inducing changes in breathing rate, inspired gas concentration, or other physiologic perturbations such as pressure, motion, or cellular metabolism. This report has been a simple step in the system development, but considering the technological challenges involved in realizing this system, the demonstration of phantom quantification and *in vivo* monitoring is a major milestone. The next phase of testing can come in systematic examination of physiological changes *in vivo*, requiring a human subject's protocol plan. Ongoing work in inspired gas changes are being tested with a system achieving 0.5 Hz acquisition,[19] and so this new system should be much more informative to track this dynamic data.

Admittedly, this NIR system requires prior information about μ_s', which is not available with the CW working mode of LDs. The pre-assumed homogeneous μ_s' of each tissue type differed from the heterogeneous nature of breast tissue, and even the mean value of μ_s' in each tissue region could offset from the pre-assumed value. However, we have verified through comprehensive simulations that heterogeneity of μ_s' has little effect on the recovered μ_a with the region-based reconstruction scheme, given the pre-assumed μ_s' is not far from the average value of the true μ_s' in the region. The reason behind this is that the recovered μ_a is also averaged with the region-based scheme, thus it suffers little from the heterogeneity of μ_s'. Overestimated μ_s' values lead to underestimated μ_a in the reconstruction, and vice versa. But it does not change the overall trends in the μ_a values, e.g., when the true μ_a reaches maximum, so does the reconstructed μ_a. Therefore this system is ideal for applications where the temporal trend of μ_a is of interest, and could readily be applied to track the clearance of optical contrast agents such as indocyanine green (ICG) and these studies are currently being planned.

The system is also well suited to monitor breast hemodynamics, such as shown in the patient experiment described herein, though the current configuration cannot recover the temporal HbO and Hb variations because of the possible offset in the pre-assumed value of μ_s'. To enable the system to

accurately monitor the breast hemodynamics, we are working on incorporating our frequency-domain NIR tomography system with six discrete measurement wavelengths[20,21] previously developed in our group, which can provide reference μ_s' and chromophore information of the breast tissue. A new breast interface will be built to accommodate fibers from both the two-wavelength NIR system and the multi-wavelength system, facilitating the measurement of all major tissue chromophores, scattering, and dynamic changes in HbO and Hb in a single imaging session.

6. Conclusions

A two-wavelength high frame-rate NIR tomography system was described which has the capability to image through thick breast tissue at 20 Hz. Its performance to recover temporal hemoglobin content and oxygen saturation with good knowledge of μ_s' was verified through tissue-like phantom experiments. The data were acquired within a clinical MR system, and an MR-compatible pulse oximeter was used in a single patient imaging experiment. Image co-registration of the NIR system and the MR system, as well as the synchronized data acquisition of the NIR system and the PO have been demonstrated. The raw data from the NIR system demonstrated the system's capacity to detect the fluctuation of optical signals caused by both breathing and the heartbeat. With pre-assumed μ_s' values of breast tissue, μ_a for two tissue types at two wavelengths were successfully recovered at 20 Hz with the region-based reconstruction scheme.

Acknowledgments

We gratefully acknowledge National Institutes of Health (NIH) research grants R33CA100984, RO1CA069544, and P01CA080139.

References

1. B. J. Tromberg, B. W. Pogue, K. D. Paulsen, A. G. Yodh, D. A. Boas, A. E. Cerussi, "Assessing the future of diffuse optical imaging technologies for breast cancer management," *Med. Phys.* **35**(6), 2443−2451 (2008).
2. D. A. Boas, K. Chen, D. Grebert, M. A. Franceschini, "Improving the diffuse optical imaging spatial resolution of the cerebral hemodynamic response to brain activationin humans," *Opt. Lett.* **29**(13), 1506−1508 (2004).
3. Q. Fang, S. A. Carp, J. Selb, G. Boverman, Q. Zhang, D. B. Kopans, R. H. Moore, E. L. Miller, D. H. Brooks, D. A. Boas, "Combined optical imaging and mammography of the healthy breast: Optical contrast derived from breast structure and compression," *IEEE Trans. Med. Imag.* **28**(1), 30−42 (2009).
4. Q. Zhu, M. Huang, N. Chen, K. Zarfos, B. Jagjivan, M. Kane, P. Hedge, H. Kurtzman, "Ultrasound-guided optical tomographic imaging of malignant and benign breast lesions: Initial clinical results of 19 cases," *Neoplasia* (New York) **5**(5), 379 (2003).
5. Q. Fang, J. Selb, S. A. Carp, G. Boverman, E. L. Miller, D. H. Brooks, R. H. Moore, D. B. Kopans, D. A. Boas, "Combined optical and X-ray tomosynthesis breast imaging," *Radiology* **258**(1), 89−97 (2011).
6. V. Ntziachristos, A. G. Yodh, M. D. Schnall, B. Chance, "MRI-guided diffuse optical spectroscopy of malignant and benign breast lesions," *Neoplasia* **4**(4), 347−354 (2002).
7. B. Brooksby, B. Pogue, S. Jiang, H. Dehghani, S. Srinivasan, C. Kogel, T. Tosteson, J. Weaver, S. Poplack, K. Paulsen, "Imaging breast adipose and fibroglandular tissue molecular signatures by using hybrid MRI-guided near-infrared spectral tomography," *Proc. Nat. Acad. Sci.* **103**(23), 8828 (2006).
8. C. M. Carpenter, R. Rakow-Penner, S. Jiang, B. W. Pogue, G. H. Glover, K. D. Paulsen, "Monitoring of hemodynamic changes induced in the healthy breast through inspired gas stimuli with MR-guided diffuse optical imaging," *Med. Phys.* **37**(4), 1638−1646 (2010).
9. S. Jiang, B. W. Pogue, C. M. Carpenter, P. A. Kaufman, K. D. Paulsen, "Near-infrared spectral tomography system for measuring dynamic vascular changes in breast," in *Biomed. Opt.*, OSA Technical Digest, paper BSuB6 (2010).
10. C. H. Schmitz, D. P. Klemer, R. Hardin, M. S. Katz, Y. Pei, H. L. Graber, M. B. Levin, R. D. Levina, N. A. Franco, W. B. Solomon, R. L. Barbour, "Design and implementation of dynamic near-infrared optical tomographic imaging instrumentation for simultaneous dual-breast measurements," *Appl. Opt.* **44**(11), 2140−2153 (2005).
11. J. Lasker, J. Masciotti, M. Schoenecker, C. Schmitz, A. Hielscher, "Digital-signal-processor-based dynamic imaging system for optical tomography," *Rev. Sci. Instrum.* **78**, 083706 (2007).
12. D. K. Joseph, T. J. Huppert, M. A. Franceschini, D. A. Boas, "Diffuse optical tomography system to image brain activation with improved spatial resolution and validation with functional magnetic resonance imaging," *Appl. Opt.* **45**(31), 8142−8151 (2006).

13. D. Piao, S. Jiang, S. Srinivasan, H. Dehghani, B. W. Pogue, "Video-rate near-infrared optical tomography using spectrally encoded parallel light delivery," *Opt. Lett.* **30**(19), 2593−2595 (2005).
14. Z. Li, V. Krishnaswamy, S. C. Davis, S. Srinivasan, K. D. Paulsen, B. W. Pogue, "Video-rate near-infrared tomography to image pulsatile absorption properties in thick tissue," *Opt. Exp.* **17**(14), 12,043−12,056 (2009).
15. Z. Li, V. Krishnaswamy, S. Jiang, S. C. Davis, S. Srinivasan, K. D. Paulsen, B. W. Pogue, "Rapid magnetic resonance-guided near-infrared mapping to image pulsatile hemoglobin in the breast," *Opt. Lett.* **35**(23), 3964−3966 (2010).
16. S. Srinivasan, B. Pogue, C. Carpenter, S. Jiang, W. Wells, S. Poplack, P. Kaufman, K. Paulsen, "Developments in quantitative oxygen-saturation imaging of breast tissue *in vivo* using multispectral near-infrared tomography," *Antioxidants and Redox Signaling* **9**(8), 1143−1156 (2007).
17. J. D. Gruber, "A high-frequency ultrasound-guided fluorescence tomography system for protoporphyrin-IX quantification within subcutaneous tumors," Dartmouth College, Hanover, NH, http://www.dartmouth.edu/∼nir/downloads/Gruber.pdf (2010).
18. H. van Staveren, C. Moes, J. van Marie, S. Prahl, M. van Gemert, "Light scattering in intralipid-10% in the wavelength range of 400−1100 nm," *Appl. Opt.* **30**(31), 4507−4514 (1991).
19. S. Jiang, B. W. Pogue, M. A. Mastanduno, K. E. Michaelsen, T. E. Frazee, K. D. Paulsen, S. P. Poplack, W. A. Wells, R. M. diFlorio-Alexander, P. A. Kaufman, "Assessing dynamic vascular changes in breast tissue in response to subject-specific hyperoxic and hypercarbic gas inhalation based upon end-tidal expiration," [to be published].
20. C. M. Carpenter, B. W. Pogue, S. Jiang, H. Dehghani, X. Wang, K. D. Paulsen, W. A. Wells, J. Forero, C. Kogel, J. B. Weaver, S. P. Poplack, P. A. Kaufman, "Image-guided optical spectroscopy provides molecular-specific information *in vivo*: MRI-guided spectroscopy of breast cancer hemoglobin, water, and scatterer size," *Opt. Lett.* **32**(8), 933−935 (2007).
21. M. A. Mastanduno, C. M. Carpenter, S. Srinivasan, S. Jiang, B. W. Pogue, K. D. Paulsen, "Three-dimensional MR-guided optical spectroscopy of the breast: Optimizing probe placement for improved image quality," in *Biomed. Opt.*, OSA Technical Digest, paper JMA78 (2010).